Journal of Sound and Vibration (1996) **198**(4), 411–427

THE DEVELOPMENT OF A DSP-BASED ACTIVE SMALL AMPLITUDE VIBRATION CONTROL SYSTEM FOR FLEXIBLE BEAMS BY USING THE LQG ALGORITHMS AND INTELLIGENT MATERIALS

M. R. Bai and G. M. Lin

Department of Mechanical Engineering, *Chiao-Tung University*, 1001 *Ta-Hsueh Road*, *Hsin-Chu*, *Taiwan*, *Republic of China*

(*Received* 12 *May* 1995, *and in final form* 3 *April* 1996)

An active vibration control system is proposed for suppressing the small amplitude random vibrations in flexible beams. Intelligent materials such as the piezoelectric ceramic PZT are used as the actuator and the piezoelectric plastic PVDF is used as the sensor. The characteristics of the physical system are identified by a parametric modelling technique. The linear quadratic Gaussian (LQG) algorithm is employed for the controller design. The controller is implemented on the basis of a floating-point digital signal processor. The experimental results obtained by using the active vibration control system show significant attenuation of white noise disturbance in the frequency range of approximately 100–800 Hz.

1. INTRODUCTION

Research interest in small amplitude vibration control has recently been observed. Vibration has various detrimental effects, even though the magnitude is small. For example, vibration may cause errors in precision measurement or machining in manufacturing of semi-conductors. Excessive vibration also makes it difficult to position a read/write head in a computer disk drive. This is especially true since the density of memory devices is increasing rapidly nowadays. Hence it is highly relevant to develop vibration control methods that are dedicated to the attenuation of small amplitude vibrations.

Vibration control techniques fall into two categories: passive and active. The former require the use of passive components such as vibration dampers and dynamic absorbers, which is conventional and is well developed [1]. However, the passive approach suffers from the major drawback of being ineffective at low frequencies. On the other hand, active control approaches provide numerous advantages; e.g., improved low frequency performance, reduction of size and weight, and programmable flexibility of design. Thus, active vibration control techniques serve as promising alternatives to conventional passive methods [2].

The aim of this study is to develop an active vibration control system for suppressing small amplitude and broadband random vibrations in flexible cantilever beams. This system integrates optimal control algorithms, intelligent materials and digital signal

0022–460X/96/490411 + 17 $25.00/0

processor technologies. Intelligent materials are employed as the transducers to convert small amplitude vibration signals into electrical signals, and vice versa. More precisely, the piezoelectric ceramic PZT is used as the actuator and the piezoelectric plastic PVDF is used as the sensor. Intelligent materials have a great variety of applications since they provide many attractive features, including light weight, high sensitivity, large bandwidth and distributed properties [3–6]. In particular, PVDF can be applied in a conformal way to the structures of irregular surfaces. Since piezoelectric transducers are essentially a distributed type of device, they can be more effective in global sensing and control than conventional transducers such as accelerometers that are operated point-wise. These useful properties make intelligent materials well suited to controlling flexible structures.

In the modelling of physical systems, analytical methods such as the modal expansion, or numerical methods such as the finite element method, are available [7]. Alternatively, an experimental approach is adopted in this study to identify the characteristics of the plant comprising the sensor, the actuator and the beam by using parametric modelling techniques [8]. The mathematical model obtained by this system identification procedure is then properly realized and reduced so that the resulting plant model is amenable to the subsequent discrete-time controller design.

There are numerous control algorithms available for designing the controller; e.g., optimal control [9], independent modal space control [10], H_∞ optimal control [11] and so forth. In this research, the linear quadratic Gaussian (LQG) algorithm is employed for the controller design [12]. The controller consists mainly of a linear quadratic state feedback regulator and a Kalman–Bucy state estimator. The controller is implemented by using a floating-point 32-bit digital signal processor (DSP).

It is well known that the difficulty of controlling flexible structures lies in the non-minimum phase behavior when the sensor and the actuator are not collocated [13]. The non-minimum phase problem will lead to undesirable effects such as sluggish response, undershoot and a non-unique magnitude–phase relationship. The property will thus impose a constraint on the achievable performance of a control system [14]. Despite this difficulty, the experimental results obtained by using the active vibration control system show significant attenuation in the frequency range up to approximately 800 Hz.

The development of the active control system based on piezoelectric transducers is parallel to the work of reference [9]. However, the main difference between this study and reference [9] lies in that only numerical results based on experimentally identified data are presented in the latter, while in this study a complete active vibration control system has been realized on the basis of a digital signal processor. In addition, only limited results of an impulse disturbance are included in reference [9], while control results of a broadband random noise (100–800 Hz) for four sensor–actuator configurations are presented in this paper. Finally, this research employs a parametric time domain identification procedure which may be more convenient and accurate for broadband disturbance than the semi-analytic equation error approach in reference [9].

2. CONTROL ALGORITHM AND SYSTEM IMPLEMENTATION

2.1. SYSTEM IDENTIFICATION

Within the linear range, the piezoelectric effect can be described in terms of reduced tensor notations by the following constitutive equations [15]:

$$S_I = s_{IJ}^E T_J + d_{Ij} E_j, \qquad D_i = e_{iJ} S_J + \varepsilon_{ij}^S E_j, \tag{1, 2}$$

where the variables E, D, S and T are the electric field strength, the electric displacement, the mechanical strain and the mechanical stress respectively. The constants s, d, e and ε are the compliance, the piezoelectric strain constant, the piezoelectric charge constant and the permitivity respectively. A superscript implies that a constant is measured with the specified physical quantity maintained constant. An upper-case subscript implies a mechanical direction, while a lower-case subscript implies an electric direction. The conventions for the co-ordinate axes associated with the subscripts are indicated in Figure 1. Among these constants, e and d dictate the direct piezoelectric effect and the inverse piezoelectric effect respectively. The piezoelectric plastic PVDF, due to its large e constants, would be a preferable material for sensors, while the piezoelectric ceramic PZT, with its high d constants, would be a preferable material for actuators. Since PZT and PVDF sheets are used to control and sense the bending motion of the beam in our problem, the most relevant piezoelectric constants are d_{31} ($=1{\cdot}17 \times 10^{-10}$ m/V in our case) and g_{31} ($=5{\cdot}4 \times 10^{-2}$ C/m in our case), where the subscripts signify the axis directions shown in Figure 1(a). PZT and PVDF can be configured as either the monomorph type or the bimorph type, as shown in Figures 1(b) and (c). In particular, the bimorph type is able

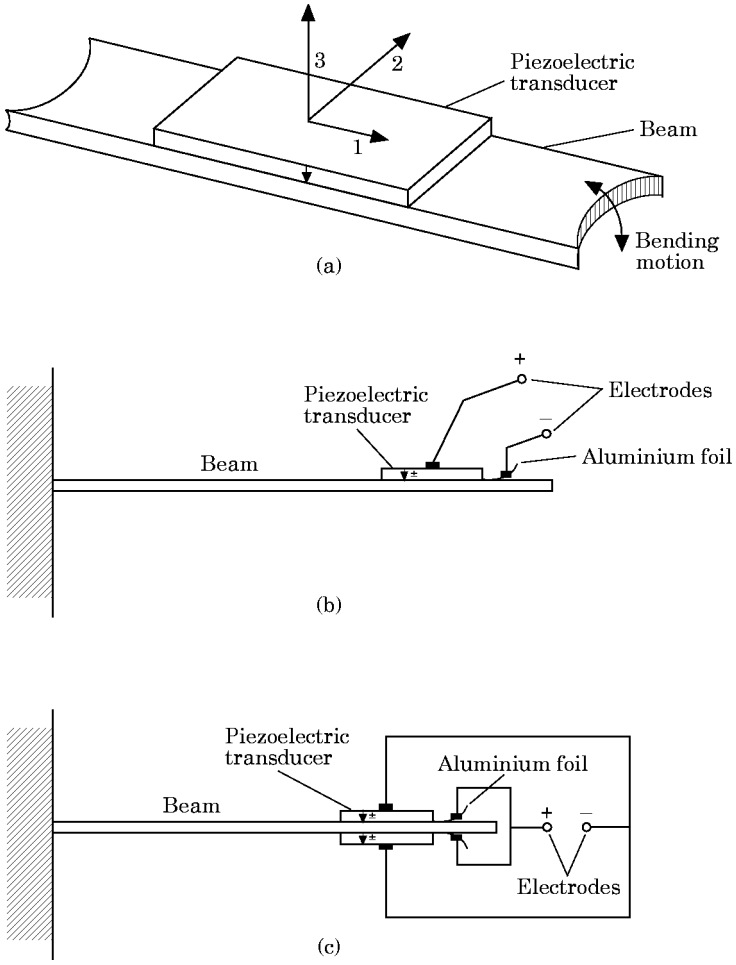

Figure 1. A schematic diagram of the transducer–beam system. (a) A piezoelectric sheet mounted on a beam and the associated convention of the co-ordinate axes; (b) a monomorph transducer; (c) bimorph transducer.

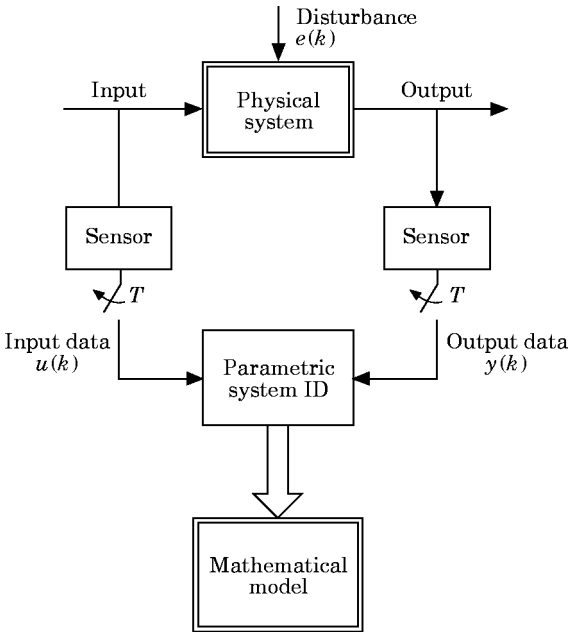

Figure 2. A schematic diagram of the parametric system identification procedure.

to create pure moment and to generate a larger actuating force than the monomorph type. The connection of electric leads subject to polarity is important for the proper operation of piezoelectric materials. It should be noted that for normal operation the PZT actuator should be boosted by a high voltage amplifier and the PVDF signal should be amplified by a charge-to-voltage converter.

It is possible to model the piezoelectric actuator and the piezoelectric sensor by analytical methods [16]. However, instead of using analytical methods, we have employed a parametric system identification procedure to establish a mathematical model of the coupled transducer–beam system [8]. This method is considered to be more universal than analytical or numerical methods, especially for complex systems, in which analytical solutions are impractical, if not impossible. Another benefit of using the system identification approach is that the structural subsystem, the transducers and the signal conditioning subsystem can all be treated as a unit without having to model each individual part analytically. In this approach, the transfer functions involved are all between electrical signals that can easily be measured by a signal analyzer. The concept of the system identification procedure is shown in Figure 2. The input signal to the system and the output signal from the system are discretized into $u(k)$ and $y(k)$, respectively, by some data acquisition system. Then, a parametric model is estimated based on these input and output data sampled in the time domain. White noise is selected as the input signal since it satisfies the condition of *persistent excitation*, as required by a reliable identification [8]. In what follows, a parametric approach, the autoregressive with exogenous input (ARX) model, will be presented. The procedures and the associated notations are standard in much of the digital control and system identification literature, and we mention only the key items needed in the development of active vibration control. An ARX model can be expressed as

$$y(k) = g(z)u(k) + h(z)e(k), \qquad k = 1, 2, \ldots, \infty, \tag{3}$$

where z is the Z-transform variable, $g(z)$ is the transfer function relating the input and the output, and $h(z)$ is the transfer function relating the disturbance and the output. In the ARX model, the transfer functions $g(z)$ and $h(z)$ take the following forms:

$$g(z) = z^{-N}B(z^{-1})/A(z^{-1}), \qquad h(z) = 1/A(z^{-1}), \tag{4}$$

where N is the delay in samples, and $A(z^{-1})$ and $B(z^{-1})$ are polynomials in z^{-1}:

$$A(z^{-1}) = 1 + a_1 z^{-1} + \cdots + a_{na} z^{-na}, \qquad B(z^{-1}) = b_1 + b_2 z^{-1} + \cdots + b_{nb} z^{-nb+1}, \tag{5}$$

with the numbers na and $nb - 1$ being the orders of the respective polynomials. Hence, the model in equation (3) can be written as

$$A(z^{-1})y(k) = B(z^{-1})u(k - nk) + e(k). \tag{6}$$

The identification procedure consists mainly of estimating these $(na + nb)$ parameters involved in the ARX model by, for example, the least-squares method. The identified single-input–single-output (SISO) model can then be realized by a state space form

$$\mathbf{x}(k + 1) = \mathbf{A}\mathbf{x}(k) + \mathbf{B}u(k), \qquad y(k) = \mathbf{C}\mathbf{x}(k) + Du(k) + e(k), \tag{7}$$

in which the coefficient matrices satisfy the associated transfer function

$$g(z) = \mathbf{C}(z\mathbf{I} - \mathbf{A})^{-1}\mathbf{B} + D. \tag{8}$$

A remark on system delay (which corresponds approximately to the first peak of the impulse response) is in order. Both equations (3) and (7) describe time-delay processes. The only difference is that equation (3) explicitly shows the effective delay as the integer N in equation (4), while equation (7) is a state-space realization of the *same* system and the effective delay is reflected as the *relative degree* $(= nb - 1 - na)$ of the corresponding transfer function $g(z)$ in equation (8). However, the cantilever beam is such a physical system with a finite boundary that it does not admit a *pure* time delay. A constraint on zero pure time delay has been incorporated into the system identification procedure by setting.

2.2. SYSTEM REALIZATION AND LQG CONTROL

Before embarking on formulation of the control algorithm, a brief discussion of the realization problem will be given. The system set-up is represented by the block diagram in Figure 3. The inputs correspond, respectively, to the disturbance $w_1(k)$ and the actuating

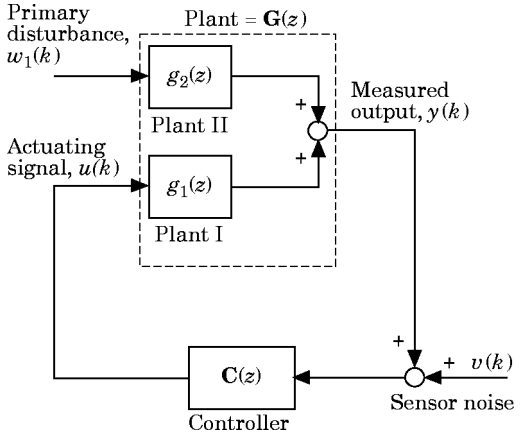

Figure 3. The realization of the two-input–one-output plant and the corresponding discrete-time closed loop system.

signal $u(k)$, while the output $y(k)$ corresponds to the signal measured by the sensor. The sensor noise is also included in the figure. The transfer functions $g_1(z)$ and $g_2(z)$ relate the actuating signal and the primary disturbance, respectively, to the sensor output. Note that all signals involved are electrical and that each subsystem contains a respective actuator, structural path and sensor. Thus, the physical system can be treated as a two-input–one-output system. Let the input–output relation be described by the following *vector* proper rational transfer function [17]:

$$\mathbf{G}(z) = [g_1(z)\ g_2(z)], \tag{9}$$

where $\mathbf{G}(z)$ is capitalized to emphasize the total system and bold-faced to indicate that it is a vector in nature. The individual scalar transfer functions $g_1(z)$ and $g_2(z)$ of the subsystems can be identified independently by using the aforementioned ARX procedure, as briefly described in equations (3)–(8). This procedure is employed to establish two discrete-time models associated with the controlling path and the disturbance path. These two subsystems can be realized in the state space representation in equation (7). These two scalar transfer functions will be assembled into a two-input–one-output vector transfer function in equation (9). Many iterations are required to ensure that a correct model for $\mathbf{G}(Z)$ is obtained, as incorrect formulation can lead to color noise being introduced in the system. In this case, the estimated parameters using the least-squares method are biased. Assume that all system poles are simple and that the *modal* statespace realizations in equation (7) for the plants $g_1(z)$ and $g_2(z)$ are expressed as

$$\mathbf{x}_1(k+1) = \mathbf{A}\mathbf{x}_1(k) + \mathbf{B}_1 u(k), \quad y_1(k) = \mathbf{C}_1\mathbf{x}_1(k) + D_1 u(k) \qquad \text{and}$$

$$\mathbf{x}_2(k+1) = \mathbf{A}\mathbf{x}_2(k) + \mathbf{B}_2 w_1(k),$$

$$y_2 = \mathbf{C}_2\mathbf{x}_2(k) + D_2 w_1(k), \tag{10}$$

where

$$\mathbf{A} = \begin{bmatrix} \lambda_1 & & & & & & & & & & \\ & \lambda_2 & & & & & & & & & \\ & & \ddots & & & & & & & & \\ & & & \lambda_K & & & & & & & \\ & & & & \sigma_1 & \omega_1 & & & & & \\ & & & & -\omega_1 & \sigma_1 & & & & & \\ & & & & & & \sigma_2 & \omega_2 & & & \\ & & & & & & -\omega_2 & \sigma_2 & & & \\ & & & & & & & & \ddots & & \\ & & & & & & & & & \sigma_L & \omega_L \\ & & & & & & & & & -\omega_L & \sigma_L \end{bmatrix}$$

$$\mathbf{B}_1 = [b_{r,1}\ b_{r,2} \cdots b_{r,K}\ b_{i,1}\ b_{i,2} \cdots b_{i,2L}]^{\mathrm{T}}, \qquad \mathbf{B}_2 = [b'_{r,1}\ b'_{r,2} \cdots b'_{r,K}\ b'_{i,1}\ b'_{i,2} \cdots b'_{i,2L}]^{\mathrm{T}},$$

$$\mathbf{C}_1 = [c_{r,1}\ c_{r,2} \cdots c_{r,K}\ c_{i,1}\ c_{i,2} \cdots c_{i,2L}]^{\mathrm{T}} \qquad \mathbf{C}_2 = [c'_{r,1}\ c'_{r,2} \cdots c'_{r,K}\ c'_{i,1}\ c'_{i,2} \cdots c'_{i,2L}]^{\mathrm{T}},$$

$$D_1 = d_1, \qquad D_2 = d_2,$$

in which the subscripts r and i denote the real part and the imaginary parts, respectively, and the primes signify the second system. The system matrices $\mathbf{A}$ in equation (10) are

finite-dimensional and identical between two subsystems because only the dominant K real poles and $2L$ complex conjugate poles that are common to both systems are retained. This appears to be a reasonable assumption, since two plants share common poles of the beam. To obtain a minimum realization of the two-input–one-output system that ensures controllability and observability is not a trivial task, because $g_1(z)$ and $g_2(z)$ share many common modes. However, a technique called Gilbert's realization enables us to accomplish the following minimum realization of the coupled system [18]:

$$\mathbf{x}(k+1) = \mathbf{A}\mathbf{x}(k) + \mathbf{B}u(k) + \mathbf{G}\mathbf{w}(k), \qquad y(k) = \mathbf{C}\mathbf{x}(k) + Du(k) + v(k), \tag{11}$$

where the matrix $\mathbf{A}$ has been defined in equation (10) and v represents the sensor noise term.

$$\mathbf{B} = \begin{bmatrix} c_{r,1}b_{r,1} \\ c_{r,2}b_{r,2} \\ \vdots \\ c_{r,K}b_{r,K} \\ \cdots\cdots\cdots\cdots\cdots \\ c_{i,1}b_{i,1} + c_{i,1}b_{i,2} \\ c_{i,1}b_{i,2} - c_{i,2}b_{i,1} \\ c_{i,3}b_{i,3} + c_{i,4}b_{i,4} \\ c_{i,3}b_{i,4} - c_{i,4}b_{i,3} \\ \vdots \\ c_{i,2L-1}b_{i,2L-1} + c_{i,2L}b_{i,2L} \\ c_{i,2L-1}b_{i,2L} - c_{i,2L}b_{i,2L-1} \end{bmatrix}_{(K+2L)\times 1}$$

$$\mathbf{G} = \mathbf{b}\mathbf{b}^{\mathrm{T}},$$

in which

$$\mathbf{b} = \begin{bmatrix} c'_{r,1}b'_{r,1} \\ c'_{r,2}b'_{r,2} \\ \vdots \\ c'_{r,K}b'_{r,K} \\ \cdots\cdots\cdots\cdots\cdots \\ c'_{i,1}b'_{i,1} + c'_{i,2}b'_{i,2} \\ c'_{i,1}b'_{i,2} - c'_{i,2}b'_{i,1} \\ c'_{i,3}b'_{i,3} + c'_{i,4}b'_{i,4} \\ c'_{i,3}b'_{i,4} - c'_{i,4}b'_{i,3} \\ \vdots \\ c'_{i,2L-1}b'_{i,2L-1} + c'_{i,2L}b'_{i,2L} \\ c'_{i,2L-1}b'_{i,2L} - c'_{i,2L}b'_{i,2L-1} \end{bmatrix}_{(K+2L)\times 1,}$$

$$\mathbf{C} = [1 \quad 1 \quad \ldots \quad 1 \quad \vdots \quad 1 \quad 0 \quad 1 \quad 0 \quad \ldots \quad 1 \quad 0]_{1\times(K+2L)}, \qquad D = d_1,$$

and

$$\mathbf{w}(k) = \frac{\mathbf{b}}{\mathbf{b}^{\mathrm{T}}\mathbf{b}}\, w_1(k).$$

Equation (11) is the statespace representation of equation (9), and it is the basis for the subsequent controller design.

In the LQG algorithm, the disturbance $\mathbf{w}(k)$ and the sensor noise $v(k)$ are both assumed to be stationary, zero-mean, Gaussian white, and to have covariance matrices satisfying

$$\mathrm{E}\{\mathbf{w}(k_1)\mathbf{w}^{\mathrm{T}}(k_2)\} = \mathbf{V}_1\delta(k_{,2} - k_1) \qquad \text{and} \qquad \mathrm{E}\{v(k_1)v(k_2)\} = V_2\delta(k_2 - k_1), \tag{12}$$

where $\mathrm{E}\{\cdot\}$ denotes the expected value, δ denotes the Kronecker delta, and $\mathbf{V}_1$ and V_2 represent, respectively, the intensities of the primary disturbance and the sensor noise, and are assumed to be positive definite. In this study, $\mathbf{V}_1 = V_1\mathbf{I}$, in which $\mathbf{I}$ is an identity the dimension of which is the same as that of the system matrix $\mathbf{A}$ and V_1 is a positive number. In addition, $\mathbf{w}(k)$ and $v(k)$ are assumed to be uncorrelated since the direct transmission terms d_1 and d_2 are generally very small, i.e.,

$$\mathrm{E}\{\mathbf{w}(k_1)v(k_2)\} = 0. \tag{13}$$

The controller consists of a state feedback module and a state estimation module. The former corresponds to the following control law:

$$u(k) = -\mathbf{K}\mathbf{x}(k), \tag{14}$$

in which $\mathbf{K}$ denotes the feedback gain vector. To determine $\mathbf{K}$, the stochastic optimal control approach [12] is employed in this study, not only because it accommodates a reasonable balance between the control error and the control effort, but also because it results in a stable system. The optimization procedure corresponds to the minimization of the following linear quadratic performance index:

$$J = \mathrm{E}\left\{\sum_{k=1}^{\infty} [\mathbf{x}^{\mathrm{T}}(k)\mathbf{Q}\mathbf{x}(k)\mathbf{Q}\mathbf{x}(k) + Ru(k)^2]\right\}, \tag{15}$$

where $\mathbf{Q}$ is a positive semi-definite matrix and R is a positive scalar. In this study, $\mathbf{Q} = Q\mathbf{I}$, in which $\mathbf{I}$ is an identity the dimension of which is the same as that of the system matrix $\mathbf{A}$ and Q is a positive number. The scalars Q and R stipulate the relative importance of the control error and control effort. A large $Q:R$ ratio corresponds to *cheap* control, while a small $Q:R$ ratio corresponds to *expensive* control. The objective of control is to regulate the system response closest to the zero state while keeping the expenditure of control energy as low a possible, by minimizing the performance index in equation (15). It can be shown that the optimal gain vector that minimizes the performance index in equation (15) reads [12]

$$\mathbf{K} = (R + \mathbf{B}^{\mathrm{T}}\mathbf{P}\mathbf{B})^{-1}\mathbf{B}^{\mathrm{T}}\mathbf{P}\mathbf{A}, \tag{16}$$

in which the positive definite matrix $\mathbf{P}$ is the solution of the following algebraic Riccati equation:

$$\mathbf{A}^{\mathrm{T}}\mathbf{P}\mathbf{A} - \mathbf{P} - \mathbf{A}^{\mathrm{T}}\mathbf{P}\mathbf{B}(R + \mathbf{B}^{\mathrm{T}}\mathbf{P}\mathbf{B})^{-1}\mathbf{B}^{\mathrm{T}}\mathbf{P}\mathbf{A} + \mathbf{Q} = \mathbf{0}. \tag{17}$$

Note that in equation (17) the steady state condition is assumed. In reality, it may not be possible to measure all of the state variables. This calls for the use of a state estimator based on the Kalman–Bucy filter:

$$\hat{\mathbf{x}}(k+1) = \mathbf{A}\hat{\mathbf{x}}(k) + \mathbf{B}u(k) + \mathbf{L}[y(k) - \mathbf{C}\hat{\mathbf{x}}(k) - Du(k)], \tag{18}$$

where $\hat{\mathbf{x}}$ denotes the estimated state and the observer gain vector is obtained from

$$\mathbf{L} = \mathbf{A}\mathbf{P}\mathbf{C}^{\mathrm{T}}(\mathbf{C}\mathbf{P}\mathbf{C}^{\mathrm{T}} + V_2)^{-1}, \tag{19}$$

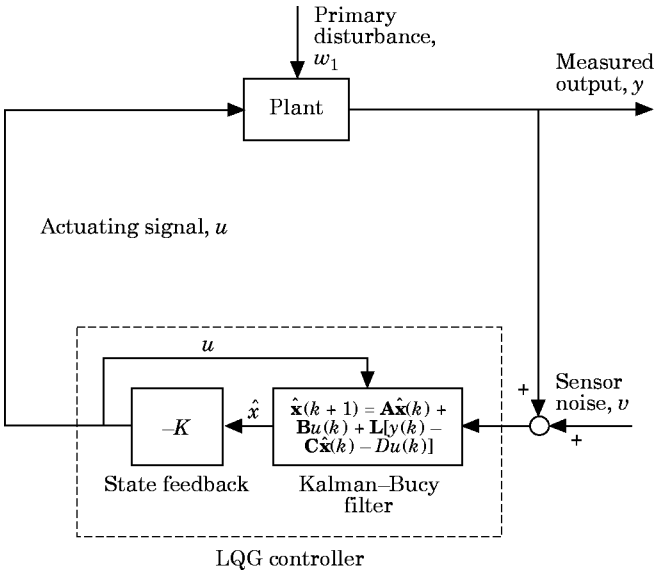

Figure 4. The general framework of the active vibration control system by using the discrete-time LQG controller.

in which the positive definite matrix $\mathbf{P}$ satisfies the following algebraic Riccati equation:

$$\mathbf{APA}^{\mathrm{T}} + \mathbf{GV}_1\mathbf{G}^{\mathrm{T}} - \mathbf{APC}^{\mathrm{T}}(\mathbf{CPC}^{\mathrm{T}} + V_2)^{-1}\mathbf{CPA}^{\mathrm{T}} - \mathbf{P} = \mathbf{0}. \tag{20}$$

Note that the state vector in equation (14) should be replaced by the estimated state $\hat{\mathbf{x}}$. One of the merits of the LQG technique lies in the *separation principle*, which states that the design of the feedback and the estimator can be carried out separately. It follows that the synthesis of the LQG controller boils down to the adjustment of the control weightings Q, R, V_1 and V_2, which requires the solution of the Riccati equations in equations (17) and (20). These two equations are of the same structure due to duality and can be solved by the eigenvector method [12]. The overall framework of the LQG controller is summarized in Figure 4. The statespace forms of the feedback and the Kalman–Bucy filter can thus be converted into transfer function forms and implemented by a digital infinite-impulse-response (IIR) filter.

3. EXPERIMENTAL INVESTIGATIONS

Experimental investigations were conducted to validate the software and the hardware of the active vibration control system. The experimental set-up is shown in Figure 5. A plastic beam of length 0·323 m, width 0·030 m, thickness 0·002 m, density $0{\cdot}587 \times 10^3$ kg/m^3 and Young's modulus $5{\cdot}33 \times 10^8$ kg/m^2 was selected for the test. The beam was cantilevered at one end and free at the other. One PZT transducer was used to generate the primary disturbance, while the other was used to generate the required control force. Both PZT transducers need high voltage power amplification. A PVDF transducer was employed as the sensor for bending motion and it required charge amplification for proper operation. The discrete time LQG controller was implemented by using a 32-bit floating-point TMS320C31 DSP board in conjunction with a 16-bit analog I/O board. The sampling rate was chosen to be 4 kHz, which gave an effective control bandwidth of approximately 800 Hz. Reducing the sampling rate would lead to degradation of

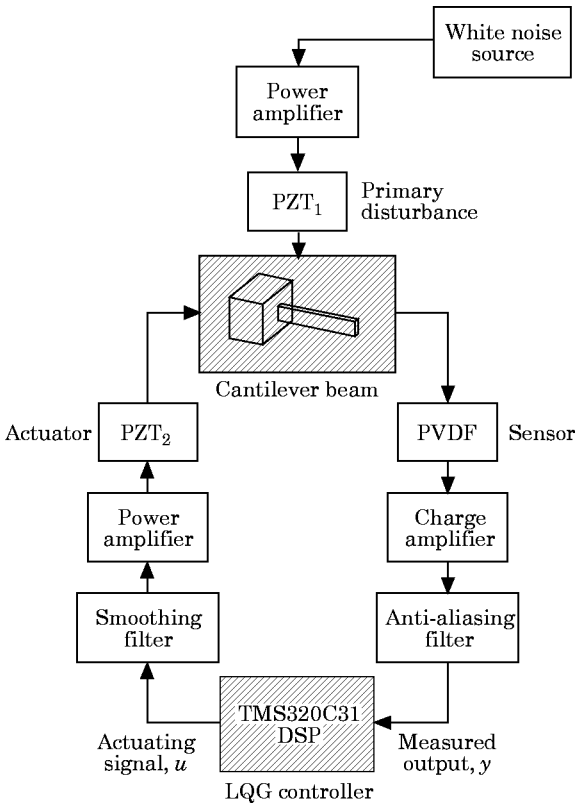

Figure 5. A schematic diagram of the experimental set-up for the DSP-based active vibration control system.

performance, whereas increasing the sampling rate further would result in difficulties in the aforementioned system identification procedure. This bandwidth includes the eight lowest modes of the cantilever beam (see Table 1 and Figure 6). Two third order Butterworth filters with a cut-off frequency of 800 Hz were used for anti-aliasing and smoothing the signals.

Four experimental cases were designed to investigate the factors that might affect the performance of the active vibration control system. The configurations of the beams and their attached sensors and actuators are shown in Figure 7 for each case. The only difference between cases 1 and 2 was the relative positions of the sensor and the actuator.

TABLE 1

Natural frequencies of the beam

Mode	Natural frequency (Hz)
1	5
2	29
3	80
4	157
5	259
6	387
7	540
8	765

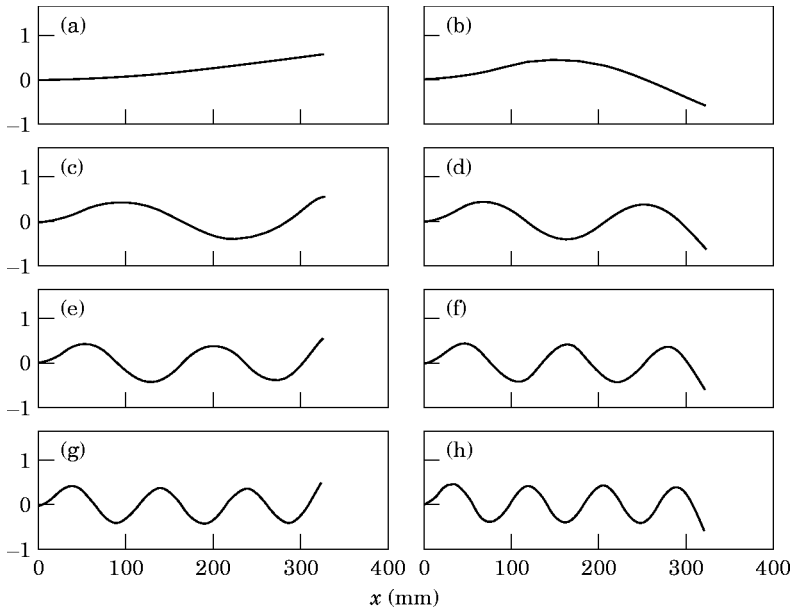

Figure 6. The mode shapes of the first eight modes of the cantilever beam. (a) Mode 1; (b) mode 2; (c) mode 3; (d) mode 4; (e) mode 5; (f) mode 6; (g) mode 7; (h) mode 8.

Hence, the same beam was used for both cases. The difference between cases 3 and 4 was the length of PVDF. The PZTs used in cases 1 and 2 were bimorphs. The PZTs used in cases 3 and 4 were monomorphs, mounted near the clamped end, which resulted in larger displacements at the free end than the other positions. The PVDFs used for all cases were monomorphs, and were mounted near the free end of the beams for good sensitivity.

For these beam–transducer systems, the aforementioned parametric identification procedure was employed to set up the corresponding mathematical models. First, white noise was used to excite the beam under test. The input data and the output data were then recorded by a signal analyzer, based on a sampling rate of 4 kHz. Second, the orders and the delay of the ARX model were adjusted. This process might take several iterations until the magnitude and the phase of the measured and the regenerated frequency response functions were well matched. The ARX model orders were selected according to the Akaike's information theoretic criterion (AIC) [8]. For example, the beam in case 1 was identified and the corresponding results are shown in Figures 8(a) and (b). The results were based on a $(na, nb, N) = (11, 9, 3)$ model for the plant $g_1(z)$ and a $(na, nb, N) = (11, 11, 4)$ model for the plant $g_2(z)$ respectively. The poles and zeros of the identified models are given in Table 2. Excellent agreement was obtained between the measured and the regenerated frequency response functions except for the frequency range below approximately 100 Hz, in which the piezoelectric transducers exhibited poor low frequency response. This further restricted the control bandwidth to 100–800 Hz, that included five vibration modes of the beam. Similarly, the mathematical models of cases 3 and 4 were calculated by using the ARX procedure. The final orders and the delays for all four cases are summarized in Table 3. The identified plant models were then realized via Gilbert's approach for the LQG design. The control weights (Q, R, V_1 and V_2) for the four cases are also listed in Table 3. It should be mentioned that the control weights were the optimal combinations achievable after several trials for each case, that gave rise to maximum attenuation within the transducer limits. The controller was then coded into a digital filter by using the digital

signal processor. Care had to be exercised to avoid some technical problems, e.g., the choice of sampling rate, aliasing prevention and the saturation problem of transducers. The experimental results obtained from the active vibration control system are presented as follows.

Case 1 is chosen as the reference case. The results for case 1 expressed in terms of the power spectrum (dB scale) of the PVDF output are shown in Figure 9. It can be seen from the comparison between the power spectrum before and after control was activated that significant attenuation (with a maximum of approximately 10 dB) was obtained at the peaks within 800 Hz. Note that the responses of the fourth mode (at 156 Hz) and the seventh mode (at 587 Hz) were smaller than those of the other modes, since the center of

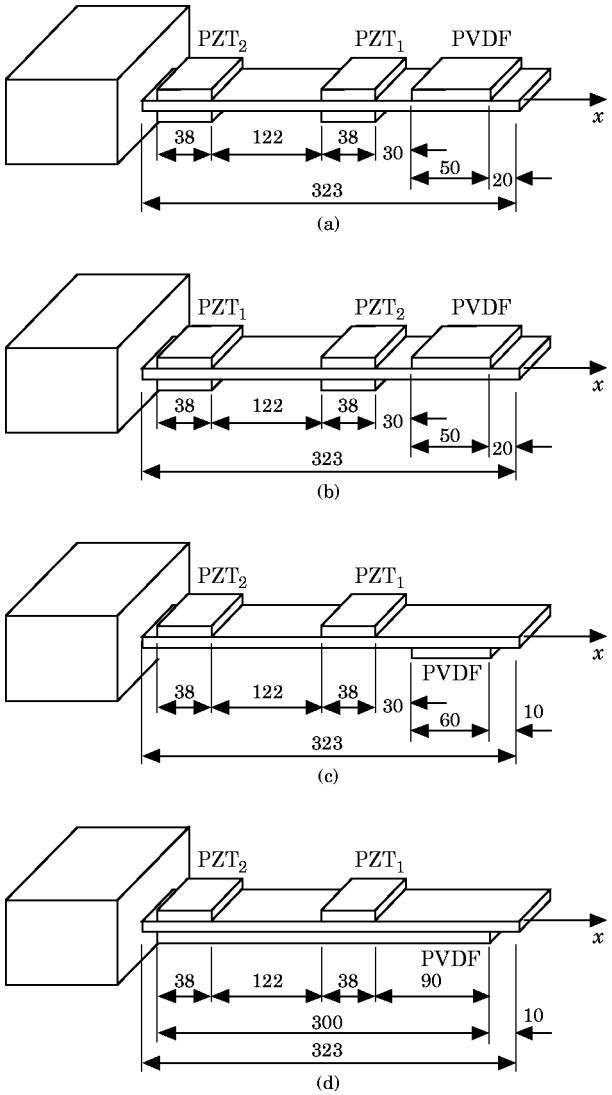

Figure 7. The configuration of the transducer–beam systems for the experimental cases. PZT_1 and PZT_2 are used to generate the disturbance and the control force, respectively. The dimensions are in millimeters. (a) case 1; (b) case 2; (c) case 3; (d) case 4.

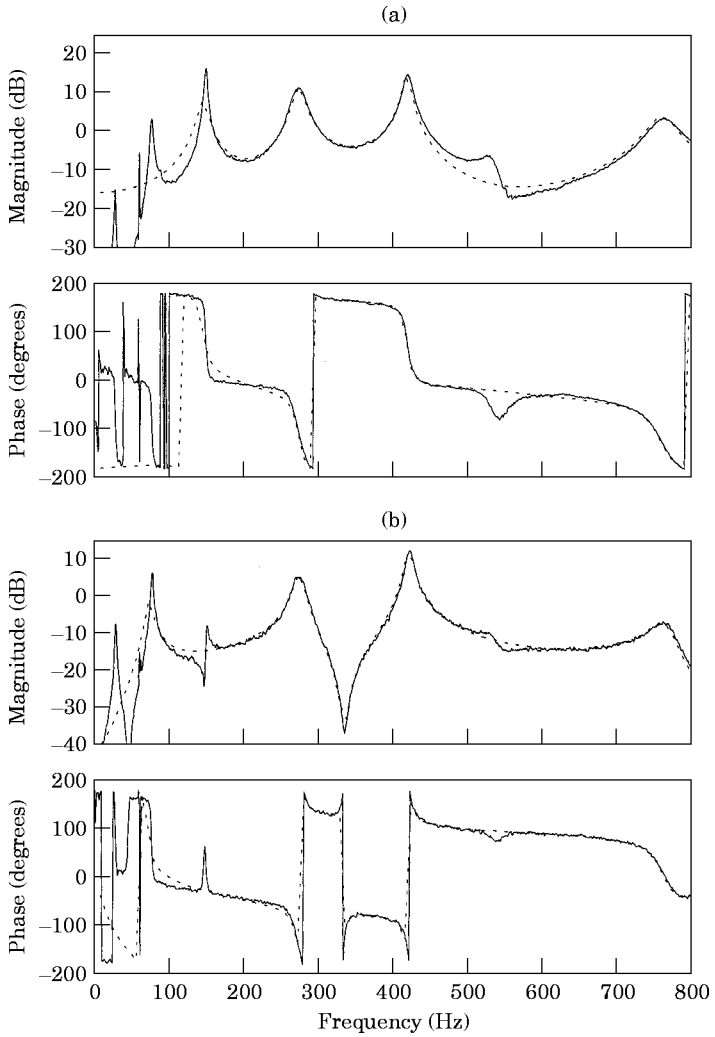

Figure 8. A comparison between the measured and the regenerated frequency response functions. (a) The frequency response function between the actuator and the sensor, $g_1(e^{j\omega})$; (b) the frequency response function between the disturbance and the sensor, $g_2(e^{j\omega})$. ——, Measured data; - - -, regenerated data.

the PVDF sheet was very near the nodal points of these modes. These two modes became almost *unobservable* to the sensor.

The purpose of case 2 is to examine the effect of collocated control. The power spectrum results for case 2 are shown in Figure 10. Attenuation was obtained for the peaks at 156 Hz, 416 Hz and 780 Hz. The control ratio of $Q:R = 10:1$ in this case was considerably smaller than the $Q:R = 1000:1$ in case 1. This can be attributed to the fact that the distance between the sensor and the actuator in case 2 was smaller than that in case 1. The situation in case 2 was close to a collocated control case, which was deemed to be easier than the non-collocated control case 1, which suffered from the non-minimum phase problem. In this case, one would be forced to increase the $Q:R$ ratio. However, one cannot increase this ratio indefinitely without eventually saturating the actuator. This difficulty was

TABLE 2

The models of $g_1(z)$ and $g_2(z)$ identified by the ARX *procedure*

$g_1(z)$		$g_2(z)$	
Zeros	Poles	Zeros	Poles
$-5{\cdot}3834$†	$-0{\cdot}8907$	$-0{\cdot}3925 \pm 1{\cdot}9421$i†	$-0{\cdot}1330$
$2{\cdot}1223$	$-0{\cdot}6440 \pm 0{\cdot}7066$i	$1{\cdot}0258 \pm 0{\cdot}7215$i†	$0{\cdot}8913 \pm 0{\cdot}4251$i
$-0{\cdot}7890 \pm 0{\cdot}5484$i	$0{\cdot}2968 \pm 0{\cdot}9377$i	$0{\cdot}0057 \pm 0{\cdot}0027$i	$0{\cdot}6708 \pm 0{\cdot}7267$i
$0{\cdot}5397 \pm 0{\cdot}8262$i	$0{\cdot}6721 \pm 0{\cdot}7262$i	$0{\cdot}0014 \pm 0{\cdot}0061$i	$0{\cdot}3007 \pm 0{\cdot}9378$i
$1{\cdot}0052 \pm 0{\cdot}1108$i	$0{\cdot}9652 \pm 0{\cdot}2254$i		$-0{\cdot}6438 \pm 0{\cdot}7072$i
	$0{\cdot}1439 \pm 0{\cdot}2100$i		$-0{\cdot}3796 \pm 0{\cdot}5834$i
Delay $N = 3$, gain $= -0{\cdot}0282$		Delay $N = 3$, gain $= -0{\cdot}0941$	

† Denotes non-minimum phase zeros.

also reflected by the fact that a smaller sensor intensity V_2 was assumed in case 2 than in case 1.

The purpose of case 3 is to investigate the active control by using monomorph transducers. The power spectrum results for case 3 are shown in Figure 11. In this case, the monomorph PZT actuator was mounted near the clamped end of the beam, so that it would create sufficient displacement at the free end. Significant attenuation was obtained for the peaks at 286 Hz and 416 Hz (approximately 10 dB and 8 dB respectively). In this case, the response of the fourth mode (at 156 Hz) was smaller than the other modes, since the center of the PVDF sheet was very near the nodal points of this mode. Note also that it required a larger $Q:R$ ratio (= 10 000:1) in case 3 than in case 1 ($Q:R = 1000:1$), since in the former case the actuator was operated in a monomorph mode.

The purpose of case 4 is to examine the increased length of the PVDF sensor. The power spectrum results for case 4 are shown in Figure 12. The major difference between this case and the last case was that the length of PVDF was considerably increased in case 4. The first to the seventh structural modes all appeared in the spectrum. Note that the responses of the odd modes were smaller than those of the other modes, since the symmetry of the mode shapes of these modes gave a smaller PVDF output, which was an averaged value along the whole sheet (see Table 1 and Figure 6). Less attenuation was achieved in case

TABLE 3

Summary of the parameters of the experimental cases

Case	Plant	(na, nb)	N	AIC	Q	R	V_1	V_2
1	$g_1(z)$	(8, 12)	3	$-3{\cdot}9$	1 000	1	$0{\cdot}2$	$0{\cdot}01$
	$g_2(z)$	(8, 12)	3	$-4{\cdot}0$				
2	$g_1(z)$	(8, 12)	3	$-4{\cdot}1$	10	1	$0{\cdot}2$	$0{\cdot}001$
	$g_2(z)$	(8, 12)	3	$-4{\cdot}0$				
3	$g_1(z)$	(7, 9)	1	$-3{\cdot}6$	10 000	1	1	$0{\cdot}1$
	$g_2(z)$	(7, 9)	1	$-3{\cdot}7$				
4	$g_1(z)$	(8, 9)	0	$-4{\cdot}5$	1	1	1	$0{\cdot}001$
	$g_2(z)$	(8, 9)	0	$-4{\cdot}4$				

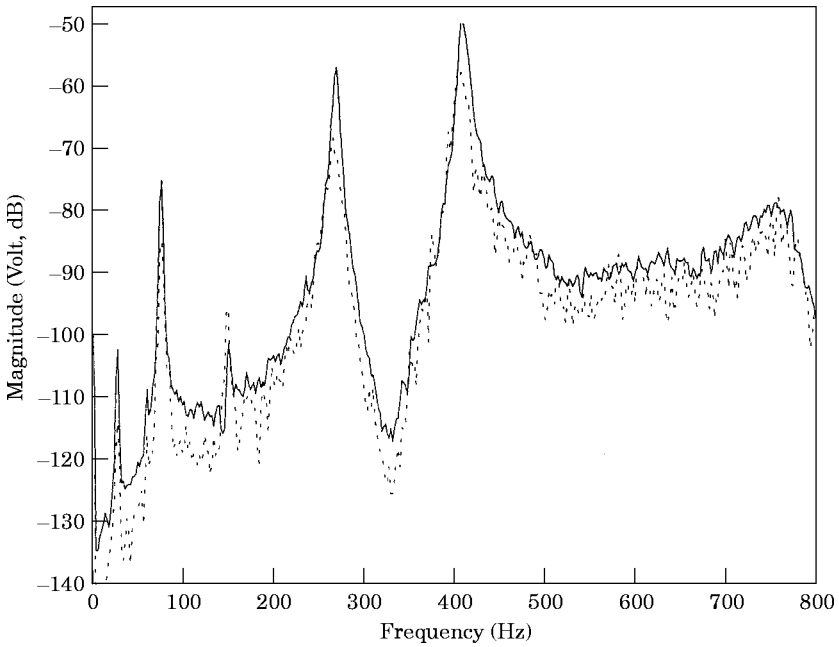

Figure 9. The experimental results of case 1 expressed in terms of the power spectrum (on a dB scale) of the PVDF output. ——, Control off; - - -, control on.

4 than in case 3. An impression may be given that a longer PVDF sheet will lead to poor attenuation. In fact, these two cases were on different bases, since the results in case 1 correspond to a local response, while the results in case 4 correspond to an averaged overall response. Nevertheless, the outcome of case 4 was still easier to achieve, as reflected by

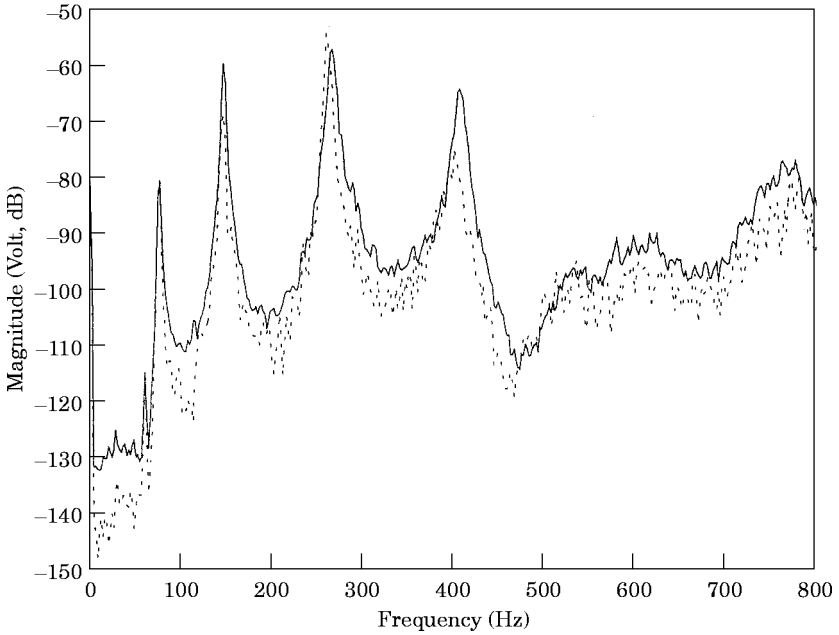

Figure 10. The experimental results of case 2 expressed in terms of the power spectrum (on a dB scale) of the PVDF output. ——, Control off; - - -, control on.

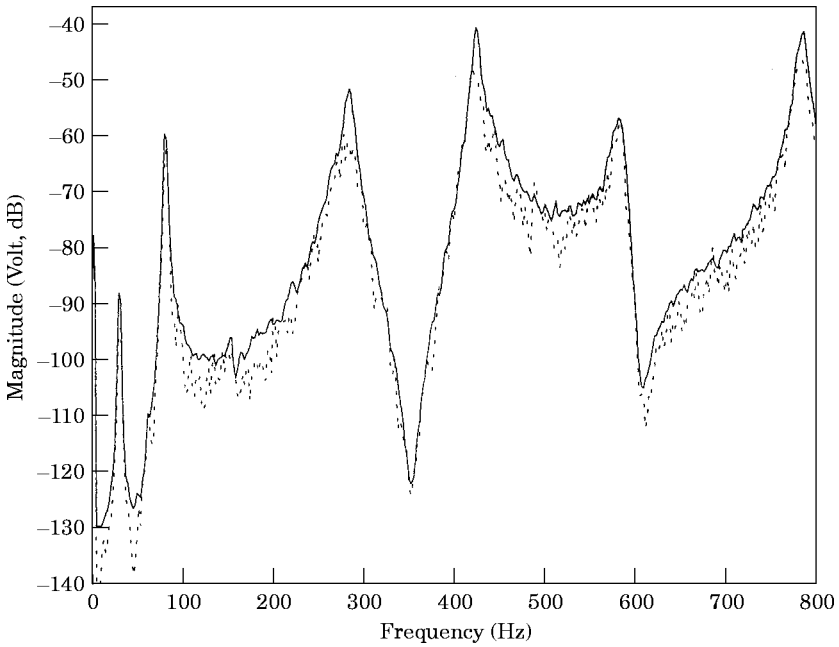

Figure 11. The experimental results of case 3 expressed in terms of the power spectrum (on a dB scale) of the PVDF output. ——, Control off; - - -, control on.

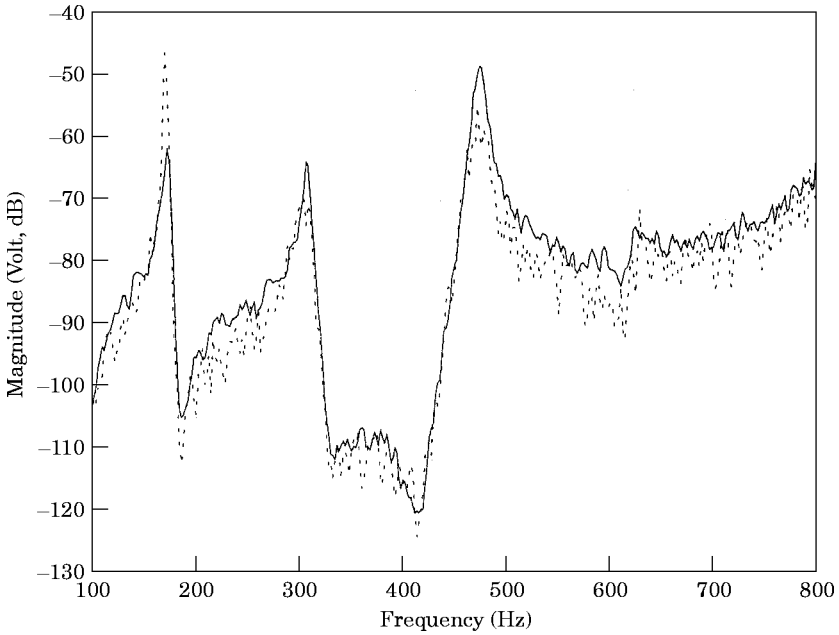

Figure 12. The experimental results of case 4 expressed in terms of the power spectrum (on a dB scale) of the PVDF output. ——, Control off; - - -, control on.

the significantly smaller control ratio ($Q:R = 1:1$ in case 4 versus $Q:R = 10\,000:1$ in case 3). The same conclusion could also be drawn by noting that a smaller sensor intensity V_2 was assumed in case 2 than in case 1.

4. CONCLUSIONS

An active vibration control system for suppressing small amplitude random vibrations in flexible beams has been developed. Intelligent materials are used as the transducers. A parametric modelling method, ARX, is employed to identify the characteristics of the physical systems. The LQG controller implemented on a floating-point DSP exhibits effectiveness in suppressing small amplitude vibrations in plastic beams. From the experimental results, it is observed that satisfactory performance of vibration attenuation can be achieved, provided that the sensor and the actuator are nearly collocated, and the PVDF sheet is of sufficient length. It should be pointed out that the method presented in this paper is limited to *regulating* control, where the reference input is zero. The applications, for example, positioning the read/write head of a disk drive, as mentioned in the Introduction, fall into the category of *tracking* control, where the reference input is not zero, and will be explored in future studies.

ACKNOWLEDGMENT

The work was supported by the National Science Council in Taiwan, Republic of China, under project number NSC 83-0401-E-009-024.

REFERENCES

1. S. S. Rao 1990 *Mechanical Vibrations*. Reading, MA: Addison-Wesley.
2. T. T. Soong 1990 *Active Structural Control*: *Theory and Practice*. New York: Longman Scientific & Technical.
3. M. V. Gandhi and B. S. Thompson 1992 *Smart Materials*. London: Chapman and Hall.
4. T. Baily and J. E. Hubbard 1985 *American Institute of Aeronautics and Astronautics*, *Journal of Guidance*, *Control and Dynamics* **8**, 605–611. Distributed piezoelectric-polymer active vibration control of a cantilever beam.
5. E. F. Crawly and J. de Luis 1985 *Proceedings of the* 26*th AIAA/ASME/ASCE/AHS Structures*, *Structural Dynamics and Materials Conference*, 126–133. Use of piezo-ceramics as distributed actuators in large space structures.
6. E. F. Crawly and J. de Luis 1987 *American Institute of Aeronautics and Astronautics*, *Piezoelectric Actuators for Intelligent Structures* **25**, 1373–1385. Use of piezoelectric actuators as elements of intelligent structures.
7. L. Meirovitch 1990 *Dynamics and Control of Structures*. New York: John Wiley.
8. L. Ljung 1987 *System Identification*: *Theory for the User*. Englewood Cliffs, NJ: Prentice-Hall.
9. S. Hanagud, M. W. Obal and A. J. Calise 1992 *American Institute of Aeronautics and Astronautics*, *Journal of Guidance*, *Control and Dynamics* **15**, 1199–1207. Optimal vibration control by the use of piezoceramic sensors and actuators.
10. L. Meirovitch and L. M. Silverberg 1983 *Optimal Control Applications and Methods* **4**, 365–386. Globally optimal control of self-adjoint distributed systems.
11. K. Lenz, H. Özbay, A. R. Tannenbaum, J. Turi and B. Morton 1991 *Automatica* **27**, 947–961. Frequency domain analysis and robust control design for an ideal flexible beam.
12. H. Kwakernaak and R. Sivan 1972 *Linear Optimal of Control Systems*. New York: John Wiley.
13. H. F. Franklin, J. D. Powell and A. Emami-Naeini 1994 *Feedback Control of Dynamic Systems*. Reading, MA: Addison-Wesley.
14. J. C. Doyle, B. A. Francis and A. R. Tannenbaum 1992 *Feedback Control Theory*. New York: Maxwell–Macmillan International.
15. G. S. Kino 1987 *Acoustic Waves*: *Devices*, *Imaging*, *& Analog Signal Processing*. Englewood Cliffs, NJ: Prentice-Hall.
16. B. T. Wang, R. A. Burdisso and C. R. Fuller 1994 *Journal of Intelligent Material Systems and Structures* **5**, 67–77. Optimal placement of piezoelectric actuators for active structural acoustic control.
17. C. T. Chen 1984 *Linear System Theory and Design*. New York: Holt, Rinehart and Winston.
18. T. Kailath 1980 *Linear Systems*. Englewood Cliffs, NJ: Prentice-Hall.